Proposal and Demonstration of Free-Space Optical Communication Using Photonic Crystal Surface-Emitting Lasers

Shota Ishimura, Ryohei Morita, Takuya Inoue, Kosuke Nishimura, Hidenori Takahashi, *Member, IEEE*, Takehiro Tsuritani, Menaka De Zoysa, Kenji Ishizaki, Masatoshi Suzuki, *Life Fellow, IEEE*, and Susumu Noda, *Fellow, IEEE*

(Post-Deadline Paper)

***Abstract*—We propose and demonstrate free-space optical (FSO) communication using photonic crystal surface-emitting lasers (PCSELs). Unlike other types of conventional semiconductor lasers, such as edge-emitting lasers (EELs) and vertical-cavity surface-emitting lasers (VCSELs), PCSELs achieve much larger area single-mode coherent lasing, and this unique feature enables high-power (>watt) and lens-free operations at the same time. To date, these advantages have been recognized to be game changing, especially in light detection and ranging (LiDAR) and laser processing applications. In this work, we show that FSO communication can also benefit from these advantages of PCSELs; more specifically, conventional transmitters that include low-power semiconductor lasers, optical lenses, and fiber-based amplifiers could be replaced with a single PCSEL. Since fiber amplifiers usually consist of bulky components and have low conversion efficiencies, PCSELs can offer more space- and power-saving solutions. Moreover, the narrow beam divergence angles directly obtained from large-area single-mode PCSELs can also eliminate the need for lens systems on the transmitter side. To experimentally verify these potential advantages, we performed FSO transmission experiments based on PCSELs and successfully transmitted 480-MHz and 864-MHz orthogonal frequency division multiplexed (OFDM) signals over 1.1 m using a 500-μm PCSEL in a lens-free transmitter configuration. We believe that PCSELs open new possibilities and choices in FSO communication.**

***Index Terms*—Free-space optical communication, orthogonal frequency division multiplexing, photonic crystal surface-emitting laser.**

Manuscript received 15 November 2022; revised 24 March 2023 and 30 April 2023; accepted 3 May 2023. Date of publication 8 May 2023; date of current version 27 June 2023. *(Shota Ishimura and Ryohei Morita contributed equally to this work.) (Corresponding authors: Shota Ishimura; Susumu Noda.)*

Shota Ishimura, Kosuke Nishimura, Hidenori Takahashi, Takehiro Tsuritani, and Masatoshi Suzuki are with the KDDI Research, Inc., Saitama 356-8502, Japan (e-mail: sh-ishimura@kddi-research.jp; nish@kddi-research.jp; takahashi@kddi-research.jp; tsuri@kddi-research.jp; suzuki@kddi-research.jp).

Takuya Inoue, Menaka De Zoysa, and Kenji Ishizaki are with the Photonics and Electronics Science and Engineering Center, Kyoto University, Kyoto 615-8510, Japan (e-mail: t_inoue@qoe.kuee.kyoto-u.ac.jp; menaka@qoe.kuee.kyoto-u.ac.jp; ishizaki@qoe.kuee.kyoto-u.ac.jp).

Ryohei Morita is with the Department of Electronic Science and Engineering, Kyoto University, Kyoto 615-8510, Japan (e-mail: moritar@qoe.kuee.kyoto-u.ac.jp).

Susumu Noda is with the Photonics and Electronics Science and Engineering Center, Kyoto University, Kyoto 615-8510, Japan, and also with the Department of Electronic Science and Engineering, Kyoto University, Kyoto 615-8510, Japan (e-mail: snoda@kuee.kyoto-u.ac.jp).

Color versions of one or more figures in this article are available at https://doi.org/10.1109/JLT.2023.3273563.

Digital Object Identifier 10.1109/JLT.2023.3273563

I. Introduction

With the ever-increasing volume of global internet data traffic, mobile data throughput has been growing exponentially, and such traffic growth has led to the evolution of mobile systems from the fourth generation (4G) to the fifth generation (5G). The 5G service offers broadband mobile communication by utilizing millimeter-wave frequency bands such as 28, 40, and 70 GHz as well as low latency and more reliability [1]. In addition, the maximum achievable throughput is expected to reach 20 Gb/s or even more. Toward beyond-5G communications, further capacity expansion has been extensively studied [2], [3], [4]; however, such massive mobile traffic is expected to put a significant burden on fiber-based mobile networks [5], [6], [7], [8], [9], e.g., backhaul and fronthaul networks. Although it is clear that conventional fiber-optic communication continues to play an important role in supporting future optical access networks, massive deployment of fiber-based mobile networks incurs operational challenges such as a lack of deployment flexibility and high installation cost. For these reasons, free-space optical (FSO) communication has been recognized as an alternative candidate to fiber-optic communication since it offers agile and flexible communication links [10], [11], [12], [13], [14], [15], [16]. In particular, urban areas can benefit from these merits of FSO communication. So far, several types of FSO communication has been proposed, such as light-emitting diode (LED)-based visible light communication (VLC) and laser-based FSO communication systems. In particular, VLC technology has recently attracted significant attention since LEDs have become more popular and accessible today [17], [18], [19]. Indeed, this technology has become recognized as Li-Fi, and its specifications are also defined by IEEE. Although VLC technology presents a wide range of applications, such as indoor [20], [21], vehicular [22], and underwater [23], [24] systems, its incoherent nature and limited modulation bandwidth make implementing high-capacity and long-distance FSO

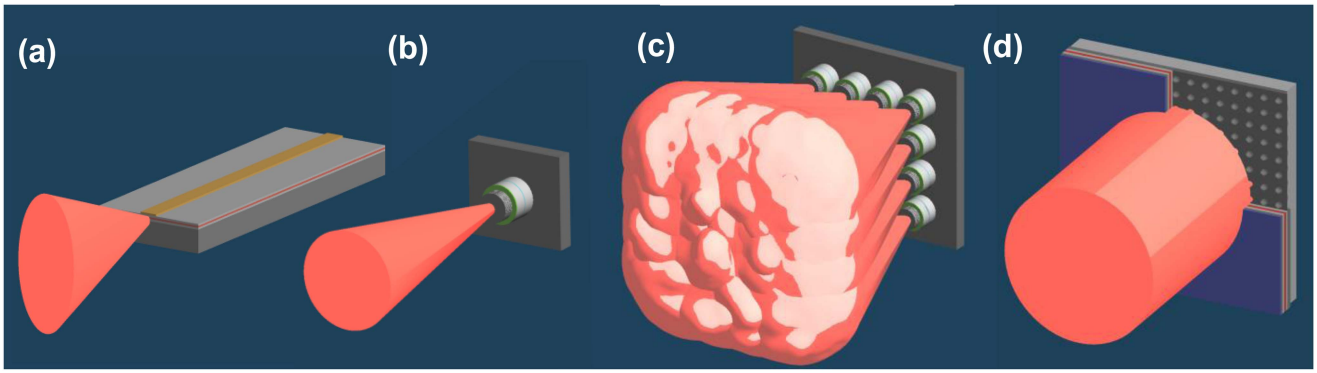

Fig. 1. Schematics of several types of semiconductor lasers: (a) EEL, (b) VCSEL, (c) VCSEL array, and (d) PCSEL.

communication systems difficult. Therefore, laser-based FSO communication is a promising candidate for beyond-5G backhaul and fronthaul networks.

One technically important factor in laser-based FSO communication is its transmitter design (e.g., the design of the lens systems and choice of the laser type) since the design determines the beam quality. Edge-emitting lasers (EELs) and vertical-cavity surface-emitting lasers (VCSELs) are common choices for FSO transmitters. Although they have been commonly used in standard fiber-optic communication [25], [26], there are still several technical challenges when they are used in FSO communication. A major issue is their poor beam quality. As shown in Fig. 1(a) and (b), both EELs and VCSELs have large output-beam divergence angles due to their small emitting apertures. The typical divergence angles for EELs and VCSELs are $\sim 5^\circ \times 30^\circ$ and $10^\circ \times 10^\circ$, respectively. Such large divergence angles lead to the need for external bulky lens systems to shape the beam profiles, which drastically increases the complexity of the transmitter. Another drawback is their low output power. The typical output powers for single-mode EELs and VCSELs are limited to $\sim$100 mW and $\sim$10 mW, respectively. Although fiber amplifiers such as erbium-doped fiber amplifiers (EDFAs) can compensate for the low output power, additional fiber coupling and amplifiers themselves increase the complexity. A VCSEL array could be another option for high-power operation, as shown in Fig. 1(c) [27], [28], [29], [30]. However, the combined light has poor beam quality due to the incoherent nature of independent light sources.

All the aforementioned issues could potentially be solved by using photonic-crystal surface-emitting lasers (PCSELs) [31]. As shown in Fig. 1(d), PCSELs can achieve single-mode coherent lasing over a large area (even $>$ mm); therefore, they can realize watt-class high-power operation while maintaining excellent beam profiles [32], which is impossible when using conventional EELs and VCSELs. Recently, PCSELs using double-lattice photonic crystals achieved an output power as high as 10 W [33] and even 29 W [34] while maintaining a low divergence angle. Such direct generation of high-power optical signals should have a higher power conversion efficiency than amplification using EDFAs, the efficiency of which is typically $\sim$10% or less. Therefore, PCSELs should be able to contribute to the deployment of power-saving FSO communication systems. In addition, since large-area lasing leads to very narrow beam divergence, PCSELs eliminate the need for an external lens system. This makes the transmitter structure simple and compact.

Although PCSELs have been developed primarily for light detection and ranging (LiDAR) systems and laser processing applications thus far [35], [36], we recently proposed and demonstrated FSO communication using a PCSEL for the first time [37]. In this paper, we describe the demonstrations of PCSEL-based FSO communication, including more detailed experimental results. We first investigate the frequency characteristics of PCSELs and demonstrate their capability of GHz-class direct modulation. Next, we investigate the applicability of PCSELs in Gb/s-class FSO communication. We successfully transmitted a 480-MHz 64-ary quadrature-amplitude-modulated (64QAM) orthogonal frequency division multiplexed (OFDM) signal over a free space of 2.6 m based on direct modulation of a continuously oscillating PCSEL with a lasing diameter of 250 μm, where we achieved a gross bit rate of 2.88 Gb/s and a corresponding net bit rate of 2.32 Gb/s. Then, we investigate the possibility of lens-free transmission in FSO communication using a PCSEL with a larger diameter of 500 μm, which enables higher power and narrower divergence angle operations. By operating this PCSEL under quasi-CW (QCW) operation and applying direct modulation to the PCSEL, we successfully transmitted 480- and 864-MHz 64QAM OFDM signals over a 1.1-m free space with a launched power of 1 W without using any lenses in the transmitter. This demonstration proves the feasibility of watt-class high-speed FSO communication using a compact and lens-free PCSEL transmitter.

This paper is organized as follows: we present the fundamental device characteristics of two types of PCSELs in Section II. Subsequently, we present two FSO transmission experiments using the PCSELs and demonstrate the possibility of lens-free 5Gb/s-class FSO communication in Section III. Then, we discuss the challenges and solutions associated with the further increase in the gross bit rate and transmission distance in Section IV. We finally summarize this paper in Section V.

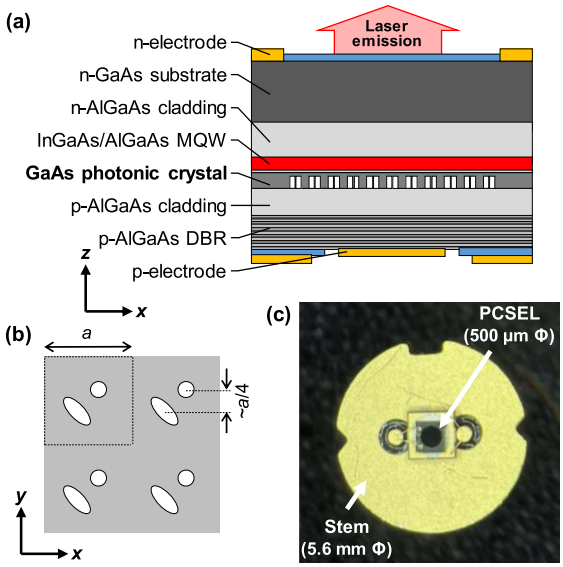

Fig. 2. (a) Cross-sectional schematic of a PCSEL. (b) Schematic structure of a double-lattice photonic-crystal. (c) External appearance of the 500-μm PCSEL packaged into a 5.6-mmφ stem.

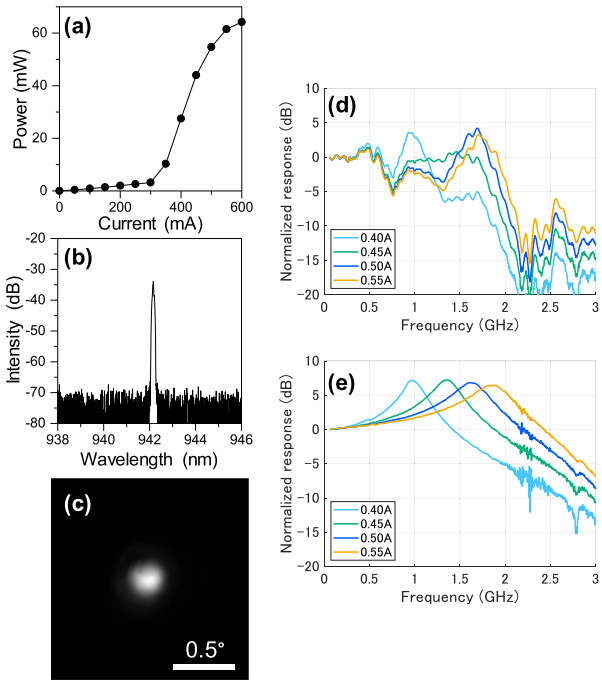

Fig. 3. Device characteristics of the 250-μm PCSEL: (a) I-L curve, (b) lasing spectrum at 520 mA, (c) far-field pattern at 500 mA, and (d) measured frequency response of the system, and (e) measured intrinsic frequency response of the PCSEL, which was obtained by subtracting the frequency response of the electrical system from the data shown in (d).

II. Device Characterizations

The PCSELs used in this work have double-lattice photonic crystal structures, which were originally proposed in [33]. The structure can effectively suppress coupling among the counter-propagating fundamental Bloch waves in a photonic crystal. As a result, the unwanted high-order modes are effectively cut off even if the PCSEL size is exceptionally large. Therefore, this structure enables PCSELs to lase with high output power while maintaining single-mode oscillation.

In this section, we present the results of the device characterization of two PCSELs: a PCSEL with a lasing diameter of 250 μm and a PCSEL with a diameter of 500 μm. The cross-sectional schematic of the device structure is shown in Fig. 2(a). The above-mentioned double-lattice photonic crystal layer [shown in Fig. 2(b)] was introduced near the active layer (InGaAs/AlGaAs triple quantum wells) and was sandwiched with p-cladding and n-cladding layers for current injection. We packaged the 250-μm and 500-μm PCSELs in 9-mmφ and 5.6-mmφ stems, respectively. The external appearance of the 500-μm PCSEL before encapsulation is shown in Fig. 2(c). During measurement, the devices were placed on commercial laser diode mounts integrated with TEC controllers and bias tees (Thorlabs LDM90 for the 250-μm PCSEL; Thorlabs LDM9T for the 500-μm PCSEL).

We first present the characterization results of the 250-μm PCSEL under DC operation. The measured I-L curve, lasing spectrum, and far-field pattern are shown in Fig. 3(a)–(c), respectively. Fig. 3(a) shows that the threshold current and slope efficiency of the PCSEL are 310 mA and ~0.3 W/A, respectively. The lower slope efficiency compared to that in our previous report (~ 0.8 W/A) [35] is due to the high thermal resistance of the commercial laser mount we used, which can be improved by better thermal management. The lasing spectrum shown in Fig. 3(b) indicates the single-mode operation with a lasing wavelength of 942.1 nm. The full width at half maximum (FWHM) of the far-field pattern is ~0.2° as shown in Fig. 3(c). We then measured the frequency response of the PCSEL using a network analyzer by changing the injection bias current. In the measurement, we applied a small radio-frequency (RF) signal from the analyzer into the RF port of the bias tee, the output beam from the PCSEL was directly injected into an InGaAs photodiode (PD), the 3-dB bandwidth of which was 4 GHz, and its electrical signal was connected to the analyzer. The raw data of the measured frequency response are shown in Fig. 3(d). We confirmed that the direct modulation of the PCSEL was possible in this system up to a frequency of 2 GHz. It should be noted that we observed dips around 700 MHz and above 2 GHz, which were caused by the frequency response of the electrical system we used (i.e., the bias tee and laser mount). To investigate the intrinsic frequency characteristics of the PCSEL itself, we subtracted the frequency response of the electrical system from these raw data. The frequency response of the electrical system was obtained by driving the PCSEL at a QCW condition with a much higher injection current (0.86 A), where the frequency response of the PCSEL is expected to flatten below 3 GHz. The results are shown in Fig. 3(e), where the increase in the relaxation oscillation frequency with the bias current was clearly observed, as is well-known in semiconductor laser theories.

Fig. 4 shows the I-L curve, far-field pattern, and frequency responses (raw data and subtracted data) of the 500-μm PCSEL. These experiments were conducted under QCW operation because the injection current of the 500-μm PCSEL (1~3 A) exceeds the allowed range of the laser mount we used. The QCW

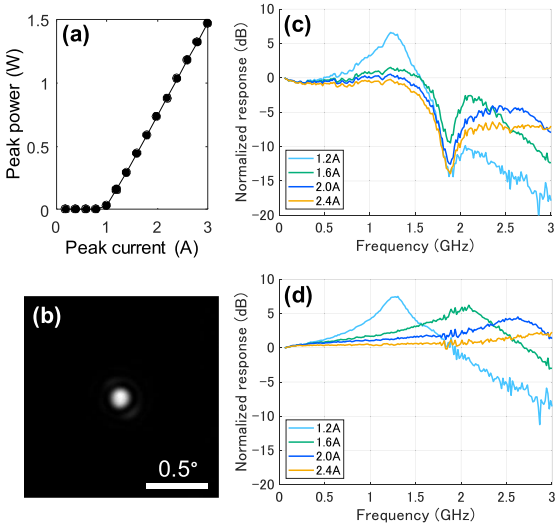

Fig. 4. Device characteristics of the 500-μm PCSEL: (a) I-L curve, (b) far-field pattern, (c) measured frequency response of the system, and (d) measured intrinsic frequency response of the PCSEL, which was obtained by subtracting the frequency response of the electrical system from the data shown in (c).

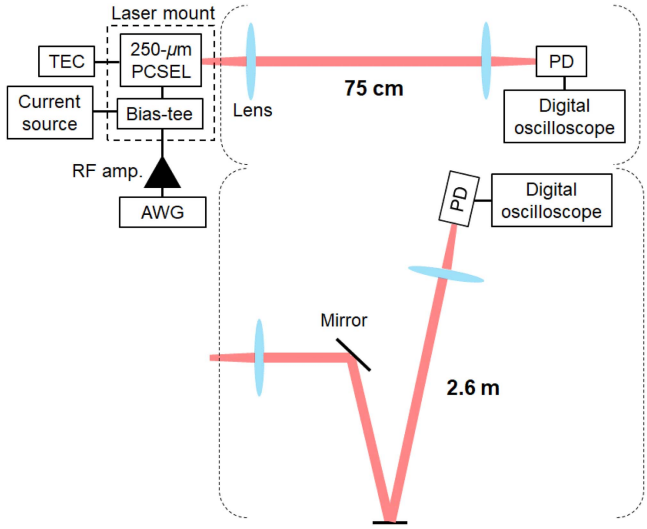

Fig. 5. Experimental setup for Gb/s-class FSO transmission. Parentheses indicate setups for two transmission scenarios: 75 cm and 2.6 m.

pulse width and repetition rate were set at 100 μs and 10 Hz, respectively (i.e., the pulse duty ratio was 0.1%). As shown in Fig. 4(a), the PCSEL shows a threshold current of $\sim$ 1.0 A, a slope efficiency of $\sim$0.7 W/A, and a peak power of $>$1 W. In Fig. 4(b), the FWHM of the beam divergence angle was observed to be $\sim$0.13°, which was smaller than that of the 250-μm PCSEL due to the larger area lasing. In the frequency response of the system shown in Fig. 4(c), we obtained almost flat frequency responses below 1.5 GHz at a bias current of 2.4 A, which is suitable for the transmission of OFDM signals. We also observed a frequency dip at $\sim$1.8 GHz, which was due to the frequency response of the bias tee in the laser mount. For the intrinsic frequency response of the PCSEL itself (Fig. 4(d)), the relaxation oscillation frequency shifted to a higher frequency side as the injected current increased, and it exceeded 3 GHz at an injection current of 2.4 A. The higher relaxation oscillation frequency obtained in the 500-μm PCSEL compared to the 250-μm PCSEL was owing to the higher injection current density of the former ($J \sim 2.4\, J_{\rm th}$, where $J_{\rm th}$ is the threshold current density) than that of the latter ($J \sim 1.8 J_{\rm th}$).

III. FSO Transmission Experiments

A. Demonstration of Gb/s-class FSO Transmission Using the PCSEL

Here, we performed FSO transmission experiments based on direct modulation of the 250-μm PCSEL to investigate the applicability of PCSELs to Gb/s-class optical communication. In this experiment, we operated the PCSEL in a CW mode by applying DC current and then applied to an RF signal to the PCSEL to perform direct modulation. The experimental setup is shown in Fig. 5. On the transmitter side, we first generated OFDM signals using offline digital signal processing (DSP). The fast Fourier transform (FFT) size and the subcarrier spacing of the OFDM signal were set at 2048 and 4 MHz, respectively. Then, we generated OFDM signals by taking 2048 inverse FFT (IFFT) of 100 data subcarriers and 20 pilot subcarriers modulated in the 64QAM format and the quadrature-phase-shift-keyed (QPSK) format, respectively. Therefore, the total bandwidth of the OFDM signal became 120 $\times$ 4 MHz = 480 MHz. The number of OFDM symbols was set at 100. The OFDM signal was subsequently sent to and generated from an arbitrary waveform generator (AWG) running at 65 GS/s. The OFDM signal was amplified using an electrical amplifier, the gain of which was 29 dB. A bias current was combined with the OFDM signal by the bias tee in the laser mount. The bias current was set at 520 mA in this experiment. Then, light emitted from the PCSEL was collimated using a lens and transmitted over free space. The beam spot size after the collimator was approximately 1 mm. In this experiment, we tested two transmission distances: 75 cm and 2.6 m. In the 2.6-m case, the light was reflected twice by mirrors to increase the transmission distance on an optical table. After being transmitted over free space and focused using another lens, the optical signal was detected using a silicon PD, the 3-dB bandwidth of which was 2 GHz. The electrical signal from the detector was captured using a real-time oscilloscope running at 40 GS/s and processed using an offline DSP. At the receiver DSP, the received OFDM signal was first converted to the frequency domain by FFT. Then, the 64QAM signals were equalized using a zero-forcing (ZF) equalizer. The transmission matrix used at the equalizing stage was estimated based on the pilot symbols. After parallel to serial conversion, we finally measured the error-vector magnitudes (EVMs).

Fig. 6(a) and (b) show the constellation plots of the 64QAM signals transmitted over 75 cm and 2.6 m, respectively. The measured EVMs were 5.6% and 6.3%. Although the signal transmitted over the longer distance had a slightly worse performance, we demonstrated FSO transmission using PCSELs for the first time with a gross bit rate of 2.88 Gb/s, i.e., 480 [MHz] $\times$ 6 [bit/s/Hz]. The corresponding net bit rate can also

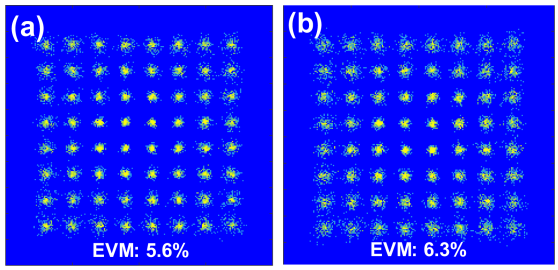

Fig. 6. Constellation diagrams of 64QAM signals transmitted over (a) 75 cm and (b) 2.6 m using the 250-μm PCSEL.

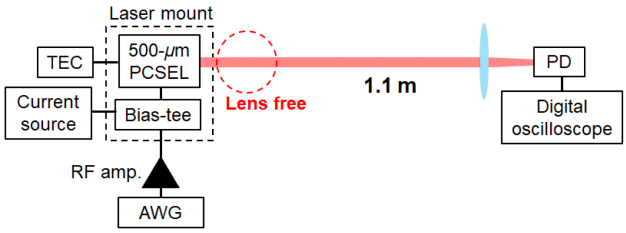

Fig. 7. Experimental setup for lens-free FSO transmission using the 500-μm PCSEL.

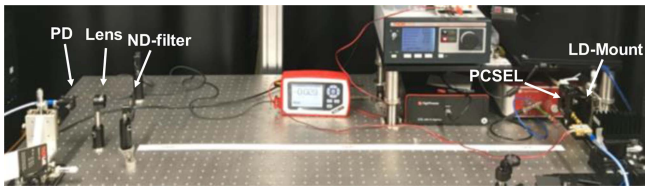

Fig. 8. Photograph of the experimental setup of lens-free FSO transmission.

be calculated by extracting the pilot symbols and the overhead of a forward-error correcting (FEC) code from the gross rate. Assuming the use of a 7%-overhead hard-decision (HD) FEC code, the net rate is calculated to be 2.32 Gb/s.

B. Demonstration of Lens-Free FSO Transmission Using the PCSEL

Motivated by the demonstration described in the previous subsection, we next performed a lens-free FSO transmission experiment using the 500-μm PCSEL, which enables higher output power and a narrower divergence angle. A schematic and photograph of the experimental setup are shown in Figs. 7 and 8, respectively. The OFDM parameters were almost the same as those used in the previous experiment. We tested two OFDM formats with different bandwidths: the first signal had the same bandwidth as in the previous experiment, while the second signal had 180 data subcarriers modulated in 64QAM and 36 pilot subcarriers modulated in QPSK. Therefore, its bandwidth was 216×4 MHz $= 864$ MHz. These OFDM signals generated from the AWG were applied to a laser mount after being amplified, as in the previous case. The peak-to-peak amplitude of the amplified signal in the 50-Ω system was estimated to be $\sim$160 mA considering the 280-mV peak-to-peak voltage of the AWG output and the amplifier gain of 29 dB. The bias current was set at 2.4 A, and the resultant peak output power was $\sim$ 1 W, as shown in Fig. 4(b). Note that the amplitude of the input RF signal was relatively small compared to the large DC bias current. This was due to the impedance mismatch between the laser mount we used and the PCSELs, where the impedance of the former was 50 Ω, while that of the latter was $\sim$0.1 Ω. It is expected that we can drastically increase the modulation depth by developing a laser mount with a tapered transmission line that can transfer the electrical power from the 50-Ω system to the 0.1-Ω system without reflection over a large bandwidth. Then, the light was emitted into the free space without using lenses and transmitted over 1.1 m.

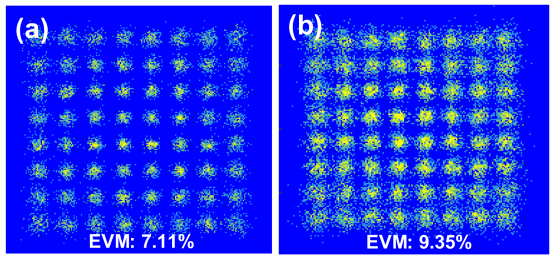

Fig. 9. Constellation diagrams of 64QAM signals with bandwidths of (a) 480 MHz and (b) 864 MHz transmitted over 1.1 m using the 500-μm PCSEL without a lens.

After being transmitted over the 1.1-m free space, the optical signal was detected using the same silicon PD. Before detection, the power was attenuated to $\sim$50 mW (13 dB attenuation) using a variable neutral density (ND) filter to emulate a long-distance free-space transmission loss. The process after signal detection was also the same as in the previous case. Fig. 9(a) and (b) show the constellation plots for the 480-MHz and 864-MHz signals, respectively. The measured EVMs were 7.11% and 9.35%. These results indicate that we can achieve lens-free FSO transmission using PCSELs with potential gross bit rates of 2.88 and 5.18 Gb/s. As with the previous demonstration, the corresponding net rates are calculated to be 2.32 and 4.17 Gb/s. Note that the transmission distance of 1.1 m was limited only by our experimental environment and could be extended further. Considering the measured far-field divergence angle (0.13°) of our 500-μm PCSEL and assuming the use of a 2-inch receiver lens for detection, the 13-dB attenuation at the ND filter in our experiment corresponds to a 100-m FSO transmission. Therefore, the maximum distance of the lens-free FSO transmission for the above device is expected to be 100 m, while maintaining 4.17 Gb/s. We should also note that the distance of the lens-free FSO transmission will be further extended by increasing the modulation depth of the PCSEL and by increasing the device size of the PCSEL, which are detailed in the next section.

IV. Discussion

In Section II, we have demonstrated the capability of GHz-class PCSEL-based direct modulation. As described there, the modulation bandwidth of the current devices is limited by the frequency response of the electrical system, such as the bias

tee and laser driver, and thus, larger modulation bandwidths (∼10 GHz) can be realized by using higher-speed laser drivers as well as the improvement of the device implementation so that the inductance and capacitance of the device can be reduced. In addition, an advanced design of the photonic crystal cavity, such as the introduction of heterostructures [38] or photon-photon resonances [39], will further increase the optical bandwidth of PCSELs above 20 GHz.

In Section III, we have demonstrated 2.88 Gb/s FSO transmission using the 250-μm-diameter PCSEL and demonstrated the possibility of 5-Gb/s-class lens-free FSO transmission using the 500-μm-diameter PCSEL. Although the latter experiment was demonstrated based on direct modulation under QCW operation in this study due to the thermal issue of the laser mount we used, the use of RF components tolerable to a high injection current will enable the lens-free demonstration under DC operation. It should also be noted that DC operation under high current injection can cause a nonuniform temperature distribution (and a nonuniform band-edge frequency distribution) inside a photonic crystal layer, which can affect the lasing characteristics of PCSELs. However, such a non-uniform effect can be mitigated by the appropriate thermal management of PCSELs [40] and compensated by introducing a temperature-compensating photonic crystal structure [41]. To further increase the modulation depth of the RF signal, it is also important to develop a laser mount that can transfer the electrical power from 50-Ω systems to low-impedance PCSELs without reflection.

Finally, we discuss the possibility of lens-free FSO transmission at longer distances, which is of great interest for practical applications such as mobile front/backhaul networks and intersatellite communication. The beam divergence angle of the 500-μm PCSEL used in this study was ∼0.1°, which corresponds to a calculated spot size of ∼20 cm after 100-m transmission. To further reduce the divergence angle to increase the signal-to-noise ratio at the receiver side, it is important to develop single-mode PCSELs with larger lasing diameters. Recently, it has been analytically shown that a proper design of double-lattice PCSELs, wherein non-Hermitian optical coupling as well as Hermitian coupling inside a photonic crystal layer is adjusted, enables >100-W output power with a device size as large as 3-10 mm while maintaining single-mode oscillation [42]. This extremely large lasing area offers a divergence angle of <0.01° and thus reduces the spot size even after 100-m and 1-km transmission to ∼1.7 cm and ∼17 cm, respectively. Therefore, it should be feasible to transmit optical signals over >1 km using such ultra large PCSELs. The use of such lens-free high-power PCSELs, instead of low-efficiency EDFAs and complex lens systems, has also the potential to significantly simplify the design of FSO transmitters for beyond-5G front/backhaul applications and intersatellite communication.

V. Conclusion

We have proposed and demonstrated lens-free FSO transmission using PCSELs for the first time. We have proposed that by using the unique features of PCSELs, such as a high output power and narrow divergence angles, we can potentially replace conventional bulky transmitters composed of fiber-based amplifiers and lenses with a single laser chip, which offers more space- and power-saving solutions. These potential advantages were experimentally verified via FSO transmission experiments. We first investigated the frequency characteristics of PCSELs and demonstrated their capability of GHz-class direct modulation. Next, we demonstrated Gb/s-class FSO transmission using a 250-μm PCSEL and demonstrated the possibility of lens-free 5 Gb/s-class FSO transmission using a watt-class PCSEL with a larger diameter of 500 μm. In the latter experiment, we could successfully transmit 480-MHz and 864-MHz OFDM signals over 1.1 m. Toward higher speed PCSEL-based FSO communication at longer distances, the development of large-area PCSELs with larger bandwidths as well as the technical improvement of the RF components and thermal management is important. We believe that these challenges can be solved in the near future and that the use of PCSELs opens new possibilities and choices in FSO communication.

References

[1] M. Shafi et al., "5G: A tutorial overview of standards, trials, challenges, deployment, and practice," *IEEE J. Sel. Areas Commun.*, vol. 35, no. 6, pp. 1201–1221, Jun. 2017.

[2] J. Zhang, E. Björnson, M. Matthaiou, D. W. K. Ng, H. Yang, and D. J. Love, "Prospective multiple antenna technologies for beyond 5G," *IEEE J. Sel. Areas Commun.*, vol. 38, no. 8, pp. 1637–1660, Aug. 2020.

[3] K. David and H. Berndt, "6G vision and requirements: Is there any need for beyond 5G?," *IEEE Veh. Technol. Mag.*, vol. 13, no. 3, pp. 72–80, Sep. 2018.

[4] I. Kanno, K. Yamazaki, Y. Kishi, and S. Konishi, "A survey on research activities for deploying cell free massive MIMO towards beyond 5G," *IEICE Trans. Commun.*, vol. 105, no. 10, pp. 1107–1116, 2022.

[5] A. Pizzinat, P. Chanclou, F. Saliou, and T. Diallo, "Things you should know about fronthaul," *J. Lightw. Technol.*, vol. 33, no. 5, pp. 1077–1083, Mar. 2015.

[6] I. A. Alimi, A. L. Teixeira, and P. P. Monteiro, "Toward an efficient C-RAN optical fronthaul for the future networks: A tutorial on technologies, requirements, challenges, and solutions," *IEEE Commun. Surv. Tut.*, vol. 20, no. 1, pp. 708–769, Firstquarter 2018.

[7] C. Ranaweera, E. Wong, A. Nirmalathas, C. Jayasundara, and C. Lim, "5G C-RAN with optical fronthaul: An analysis from a deployment perspective," *J. Lightw. Technol.*, vol. 36, no. 11, pp. 2059–2068, Jun. 2018.

[8] M. Suzuki et al., "Optical and wireless integrated technologies for future mobile networks," in *Proc. 19th Int. Conf. Transparent Opt. Netw.*, 2017, pp. 1–4.

[9] S. Ishimura, A. Bekkali, K. Tanaka, K. Nishimura, and M. Suzuki, "1.032- tb/s CPRI-equivalent rate IF-over-fiber transmission using a parallel IM/PM transmitter for high-capacity mobile fronthaul links," *J. Lightw. Technol.,* vol. 36, no. 8, pp. 1478–1484, Apr. 2018.

[10] E. Ciaramella et al., "1.28-Tb/s (32 × 40 Gb/s) free-space optical WDM transmission system," *IEEE Photon. Technol. Lett.*, vol. 21, pp. 1121–1123, 2009.

[11] D. Y. Song et al., "4 × 10 Gb/s terrestrial optical free space transmission over 1.2 km using an EDFA preamplifier with 100 GHz channel spacing," *Opt. Exp.*, vol. 7, pp. 280–284, 2000.

[12] K. Matsuda et al., "Field demonstration of real-time 14 Tb/s 220 m FSO transmission with class 1 eye-safe 9-aperture transmitter," in *Proc. Opt. Fiber Commun. Conf.*, 2021 Paper F3C.2 PDP.

[13] T. Koonen, "Indoor optical wireless systems: Technology, trends, and applications," *J. Lightw. Technol.*, vol. 36, no. 8, pp. 1459–1467, Apr. 2018.

[14] J. Wang et al., "Terabit free-space data transmission employing orbital angular momentum multiplexing," *Nature Photon.*, vol. 6, pp. 488–496, 2012.

[15] H. Huang et al., "100 Tbit/s free-space data link enabled by three dimensional multiplexing of orbital angular momentum, polarization, and wavelength," *Opt. Lett.*, vol. 39, pp. 197–200, 2014.

[16] A. Bekkali, H. Fujita, and M. Hattori, "New generation free-space optical communication systems with advanced optical beam stabilizer," *J. Lightw. Technol.*, vol. 40, no. 5, pp. 1509–1518, Mar. 2022.

[17] P. H. Pathak, X. Feng, P. Hu, and P. Mohapatra, "Visible light communication, networking, and sensing: A survey, potential and challenges," *IEEE Commun. Surv. Tut.*, vol. 17, no. 4, pp. 2047–2077, Fourthquarter 2015.

[18] N. Chi, Y. Zhou, Y. Wei, and F. Hu, "Visible light communication in 6G: Advances, challenges, and prospects," *IEEE Veh. Technol. Mag.*, vol. 15, no. 4, pp. 93–102, Dec. 2020.

[19] L. E. M. Matheus, A. B. Vieira, L. F. M. Vieira, M. A. M. Vieira, and O. Gnawali, "Visible light communication: Concepts, applications and challenges," *IEEE Commun. Surv. Tut.*, vol. 21, no. 4, pp. 3204–3237, Fourthquarter 2019.

[20] K. D. Dambul, D. C. O'Brien, and G. Faulkner, "Indoor optical wireless MIMO system with an imaging receiver," *IEEE Photon. Technol. Lett.*, vol. 23, no. 2, pp. 97–99, Jan. 2011.

[21] K. Lee, H. Park, and J. R. Barry, "Indoor channel characteristics for visible light communications," *IEEE Commun. Lett.*, vol. 15, no. 2, pp. 217–219, Feb. 2011.

[22] I. Takai et al., "Optical vehicle-to-vehicle communication system using LED transmitter and camera receiver," *IEEE Photon. J.*, vol. 6, no. 5, Oct. 2014, Art. no. 7902513.

[23] G. Cossu et al., "Experimental demonstration of high speed underwater visible light communications," in *Proc. 2nd Int. Workshop Opt. Wireless Commun.*, 2013, pp. 11–15.

[24] M. V. Jamali, J. A. Salehi, and F. Akhoundi, "Performance studies of underwater wireless optical communication systems with spatial diversity: MIMO scheme," *IEEE Trans. Commun.*, vol. 65, no. 3, pp. 1176–1192, Mar. 2017.

[25] L. A. Colderen, S. W. Corzine, and M. L. Mashanovitch, *Diode Lasers and Photonic Integrated Circuits*. Hoboken, NJ, USA: Wiley, 2012.

[26] C. J. Chang-Hasnain, J. P. Harbison, G. Hasnain, A. C. Von Lehmen, L. T. Florez, and N. G. Stoffel, "Dynamic, polarization, and transverse mode characteristics of vertical cavity surface emitting lasers," *IEEE J. Quantum Electron.*, vol. 27, no. 6, pp. 1402–1409, Jun. 1991.

[27] M. E. Warren et al., "Low-divergence high-power VCSEL arrays for lidar application," *Proc. SPIE*, vol. 10552, 2018, Art. no. 105520E.

[28] N. Haghighi, P. Moser, and J. A. Lott, "Power, bandwidth, and efficiency of single VCSELs and small VCSEL arrays," *IEEE J. Sel. Topics Quantum Electron.*, vol. 25, no. 6, Nov./Dec. 2019, Art. no. 1700615.

[29] R. Safaisini, J. R. Joseph, and K. L. Lear, "Scalable high-CW-power high-speed 980-nm VCSEL arrays," *IEEE J. Quantum Electron.*, vol. 46, no. 11, pp. 1590–1596, Nov. 2010.

[30] S. Liverman, H. Bialek, A. Natarajan, and A. X. Wang, "VCSEL array-based gigabit free-space optical femtocell communication," *J. Lightw. Technol.*, vol. 38, no. 7, pp. 1659–1667, Apr. 2020.

[31] M. Imada, S. Noda, A. Chutinan, T. Tokuda, M. Murata, and G. Sasaki, "Coherent two-dimensional lasing action in surface-emitting laser with triangular-lattice photonic crystal structure," *Appl. Phys. Lett.*, vol. 75, pp. 316–318, 1999.

[32] K. Hirose, Y. Liang, Y. Kurosaka, A. Watanabe, T. Sugiyama, and S. Noda, "Watt-class high-power, high-beam-quality photonic-crystal lasers," *Nature Photon.*, vol. 8, pp. 406–411, 2014.

[33] M. Yoshida et al., "Double-lattice photonic-crystal resonators enabling high-brightness semiconductor lasers with symmetric narrow-divergence beams," *Nature Mater.*, vol. 18, pp. 121–128, 2019.

[34] S. Katsuno et al., "29-W continuous-wave operation of photonic-crystal surface-emitting laser (PCSEL)," in *Proc. IEEE 27th Int. Semicond. Laser Conf.*, 2021, pp. 1–2.

[35] M. Yoshida et al., "Photonic-crystal lasers with high-quality narrow-divergence symmetric beams and their application to LiDAR," *J. Phys. Photon.*, vol. 3, 2021, Art. no. 022006.

[36] S. Noda, "Progress of photonic crystal surface-emitting lasers: Paradigm shift for LiDAR sensing and laser processing," *Proc. SPIE*, vol. 11672, 2021, Art. no. 1167203.

[37] S. Ishimura et al., "Proposal and demonstration of free-space optical communication using lens-free photonic-crystal surface-emitting laser," in *Proc. Eur. Conf. Opt. Commun.*, 2022, Paper Th3A.7.

[38] T. Inoue et al., "Design of photonic-crystal surface-emitting lasers with enhanced in-plane optical feedback for high-speed operation," *Opt. Exp.*, vol. 28, pp. 5050–5057, 2020.

[39] G. Morthier, R. Schatz, and O. Kjebon, "Extended modulation bandwidth of DBR and external cavity lasers by utilizing a cavity resonance for equalization," *IEEE J. Quantum Electron.*, vol. 36, no. 12, pp. 1468–1475, Dec. 2000.

[40] M. D. Zoysa et al., "Thermal management for CW operation of large-area double-lattice photonic-crystal lasers," *J. Opt. Soc. Amer. B*, vol. 37, pp. 3882–3887, 2020.

[41] S. Katsuno, T. Inoue, M. Yoshida, M. De Zoysa, K. Ishizaki, and S. Noda, "Self-consistent analysis of photonic-crystal surface-emitting lasers under continuous-wave operation," *Opt. Exp.*, vol. 29, pp. 25118–25132, 2021.

[42] T. Inoue et al., "General recipe to realize photonic-crystal surface-emitting lasers with 100-W-to-1-kW single-mode operation," *Nature Commun.*, vol. 13, 2022, Art. no. 3262.